Coulomb-influenced collisions in aerosols and dusty plasmas

Ranganathan Gopalakrishnan and Christopher J. Hogan, Jr.

Phys. Rev. E **85**, 026410 — Published 27 February 2012

DOI: 10.1103/PhysRevE.85.026410

Coulomb-Influenced Collisions in Aerosols and Dusty Plasmas

Ranganathan Gopalakrishnan & Christopher J. Hogan Jr.*

Department of Mechanical Engineering, University of Minnesota, Minneapolis, MN, USA

Submitted to:

Physical Review E

***To whom correspondence should be addressed: hogan@me.umn.edu, Tel: 1-612-626-8312, Fax: 1-612-625-6069**

ABSTRACT

In aerosol and dusty plasma systems, the behavior of suspended particles (grains) is often strongly influenced by collisions occurring between ions and particles, as well as between particles themselves. In determining the collision kernel/collision rate coefficient for such charged entities, complications arise in that the collision process can be completely described neither by continuum transport mechanics nor by free molecular (ballistic) mechanics, i.e. collisions are transition regime processes. Further, both the thermal energy and the potential energy between colliding entities can strongly influence the collision rate and must be considered. Flux matching theory, originally developed by Fuchs, is frequently applied for calculation of collision rate coefficients under these circumstances. However, recent work suggests that crucial assumptions in flux matching theory are not appropriate to describe transition regime collisions in the presence of potential interactions. Here, we combine dimensional analysis and mean first passage time calculations to infer the collision kernel between dilute charged entities suspended in a light background gas at thermal equilibrium. The motion of colliding entities is described by a Langevin equation, and Coulombic interactions are considered. It is found that the dimensionless collision kernel for these conditions, H, is a function of the diffusive Knudsen number, $\mathrm{Kn_D}$ (in contrast to the traditional Knudsen number), and the potential energy to thermal energy ratio, Ψ_E. For small and large $\mathrm{Kn_D}$, it is found that the dimensionless collision kernels inferred from mean first passage time calculations collapse to the appropriate continuum and free molecular limiting forms, respectively. Further, for repulsive collisions (Ψ_E negative) or attractive collisions with $\Psi_E < 0.5$, calculated results are in excellent agreement with flux matching theory predictions, and the dimensionless collision kernel can be determined conveniently via use of the $H(\mathrm{Kn_D})$ relationship found for hard-sphere collisions with

modified definitions of H and Kn_D to account for potential energy. However, for $\Psi_E > 0.5$, it is found that flux matching theory predictions substantially underestimate the collision kernel. We find that the collision process in this regime is governed by the minimum of Kn_D and Kn_Ψ ($Kn_\Psi = 3Kn_D/2\Psi_E$), and based on calculations, propose a function $H(Kn_D, Kn_\Psi)$ for collision kernel evaluation. The situations for which $\Psi_E > 0.5$ apply to singly charged nanoparticles and multiply charged submicrometer and supermicrometer particles, and are thus prevalent in both aerosol and dusty plasma environments.

I. INTRODUCTION

Gas phase collisions of charged particles with ions as well as with other charged particles play an important role in governing the behavior of aerosols[1-8] and dusty plasmas[9-17], with particle charge distributions in these systems dependent on the rates at which these collisions occur. Determination of the collision rates of charged entities is therefore essential in characterizing the properties and behavior of aerosol and dusty plasma particles. Under most circumstances, colliding entities are sufficiently dilute such that the collision rate, R (the number of collisions per unit volume per unit time), can be described by the following equation:

$$R = \beta n_i n_j \tag{1}$$

where n_i and n_j denote the number concentrations of colliding entities of type i and j, respectively, and β is the collision kernel, which is determined by the physics governing the collision process and is the key parameter governing the behavior of a dilute, collision-controlled system. Collisions are influenced by both the thermal energy and the potential energy between colliding entities; thus, both energies need to be considered in evaluating collision kernels. Along these lines, a number of approaches have been adopted to derive collision kernel expressions. For collisions involving at least one entity which is large in size relative to the collision persistence distance (the average straight line distance an entity in the gas phase travels due to thermal motion[18-19]), continuum approximations are valid and the influence of both the thermal energy and the potential energy can be accounted for using the approach of Fuchs[20-22], in which the collision kernel is evaluated as the product of the Smoluchowki hard-sphere collision kernel[23] and an enhancement factor, determined by the variation in potential energy with distance between colliding entities. Conversely, when both entities are extremely small relative to the collision persistence distance, free molecular mechanics best describe collisions. Under these

circumstances as well, the collision kernel can be expressed as the product of the hard sphere collision kernel and a potential energy-determined enhancement factor (different than the continuum enhancement factor)[24]. More specifically, for free molecular colliding entities interacting via a monotonic potential function which is finite at contact (e.g. the Coulomb potential), the collision kernel can be evaluated using orbital motion limited (OML) theory[25], while more involved analysis is required for singular contact potentials[24, 26-27].

Invariably, circumstances arise (e.g. systems with nanoparticles and submicrometer particles at atmospheric pressure) in which the sizes of the colliding entities are neither substantially larger nor substantially smaller than the persistence distance. In this regime, termed the transition regime, both continuum and free molecular approaches fail to correctly predict collision kernels. The first and most prevalently used method to determine collision kernels in this intermediate range is the flux matching theory, also proposed by Fuchs[1, 20, 28], primarily for the analysis of aerosol systems. In flux matching, when the colliding entities are far from one another, their motion is described by continuum mechanics (inertialess motion with diffusion), while, when the radial distance between the entities is less than a critical "limiting sphere radius"[29-30], motion obeys free molecular mechanics (ballistic motion). On the surface of the limiting sphere (centered on one of the colliding partners), the flux of incoming entities from the outer continuum is equated with their flux into the inner free molecular region, which allows for calculation of the collision kernel. The first incarnations of flux matching theory were applied in the absence of potential interactions (hard sphere collisions). With an appropriate definition of the limiting sphere radius[1, 29-30], hard sphere flux matching predictions are in good agreement with more rigorous theoretical analysis of hard sphere collisions[31], involving solution to the Boltzmann equation[32-33], the Fokker-Plank equation[34-35], and Brownian dynamics calculations[19,

[36-37]. Further, flux matching predicted hard sphere collision kernels are in reasonable agreement with experimentally measured transition regime collision rates for uncharged particles[38-39], vapor molecule uptake rates by particles[4], as well as with measurements of transition regime evaporation rates of vapor molecules from liquid drops[40]. The convergence of nearly all theoretical and experimental approaches to a single collision kernel expression suggests that at present, there is high confidence in the flux-matching derived collision kernel in the transition regime for non-interacting entities[19, 31].

Several researchers (again beginning with Fuchs[1]) have further applied flux matching theory to transition regime collisions in the presence of both thermal energy and potential energy[24, 41-42]. Most examinations along these lines focus on collisions between particles and ions, in which the combined Coulomb-image potential is considered[3], or between oppositely charged particles, considering the simple Coulomb potential[43]. As with hard-sphere collisions, predictions from alternative approaches to examine particle-ion interactions[35, 44-45] and the results of experimental studies of charged entity collisions in aerosols[3, 43, 46-49] are in good agreement with flux matching predictions. Because of its success in these instances, flux matching theory is widely accepted in aerosol science as an appropriate method for the calculation of transition regime collision rates. Moreover, quantitative size distribution measurements of submicrometer and nanometer sized particles (via electrical mobility based instruments), which are crucial in atmospheric sciences, currently depend upon flux-matching predictions of particle-ion collision kernels[50], further amplifying the importance of correct collision kernel calculation.

Unlike the study of aerosols, in the study of dusty plasmas, flux-matching has only recently been used to describe collisions between ions and charged particles (referred to in most works in dusty plasmas as grains). Apparently unaware of the precedent of Fuchs[1] and the

subsequent efforts of others[3, 24, 41-42, 51], to determine the collision rate between ions and dusty plasma grains, D'yachkov et al[52] redeveloped flux-matching theory for collisions in the presence of thermal energy and potential interactions, only differing from the original theory slightly in that D'yachkov et al: (1) assumed a slightly different limiting sphere radius, (2) considered the Coulomb potential between colliding entities as opposed to a Coulomb-image potential, and (3) considered entities crossing the limiting-sphere to be moving with a Maxwell-Boltzmann velocity distribution, as opposed to Fuchs's assumption that all entities travel at the mean thermal speed. Contrary to the conclusions found in examinations of aerosols, Gatti and Kortshagen[53] report that flux-matching predictions of the steady-state charge level of plasma grains consistently overpredict the negative charge on plasma grains, which in turn implies that flux matching theory underpredicts the (positive) ion- (negatively) charged particle collision kernel. As a simple alternative, they have proposed an analytical model in which a linear combination of continuum, free molecular, and transition regime collisions (i.e. three body trapping[42], not considered in the standard flux matching approach) are accounted for. This model, however, fails to recover the correct collision kernel for hard-spheres, and in its derivation the influence of thermal energy in the continuum regime was omitted.

In addition to the evidence provided by Gatti and Kortshagen, a closer examination of reported measurements[3, 46-49] of charged particle-ion collisions in aerosol systems reveals that although most prior works conclude that the flux matching predictions agree well with measurements, it would be more appropriate to conclude that the predictions of flux matching theory "can be fit" to experimental data. Essential to calculating the collision kernel is a priori knowledge of the mass and friction factor (inverse mobility or thermal energy/diffusion coefficient) of both colliding entities. In the case of aerosol particle-ion collisions, there are

distributions of ions mass and friction factor[54], and these ion properties have not thus far been measured directly; rather, for a set of experimental data, a single ion mass and friction factor have been inferred from simple correlations and used for comparison to theoretical predictions[3, 46]. Further, the good agreement of experimental measurements as well as alternative theoretical predictions[35] with flux matching predictions in aerosols is generally found only when the ratio of the potential energy between colliding entities to the thermal energy (Ψ_E) is less than unity. In dusty plasmas, where disagreement is found, Ψ_E is often in the 2-4 range[13]. Therefore, while flux-matching permits calculation of the transition regime collision kernel reliably when $\Psi_E = 0$, its validity for collisions in the presence of potential interactions is in question.

Given the importance of charged entity collisions in gas phase systems, there is a clear need for further examination of the transition regime collision kernel with potential interactions between colliding entities by alternative means to flux matching theory. Recently, our group has utilized a combination of mean first passage time calculations[55] and dimensional analysis to develop a non-dimensionalized functional form for the hard-sphere transition regime collision kernel[19, 56]. Here, we utilize this approach to examine collisions between spherical entities suspended in a light background gas (relative to the masses of the spheres), which are interacting with one another via a Coulombic potential. Results of our analysis are compared to the predictions of flux matching theory[52] and to a modified form of the analytical expression of Gatti and Kortshagen[53]. In the subsequent sections, the dimensional analysis is outlined, first for determining the hard-sphere collision kernel and second for the collision kernel accounting for both thermal and Coulombic energy. Next, the mean first passage time approach is outlined for determination of transition regime collision kernels and results are presented from these calculations. It is then shown that flux matching theory does not correctly predict collision

kernels for sufficiently large Ψ_E, and that collisions in the transition regime can be subdivided into three regimes: (1) the near-hard sphere regime, (2) the potential-enhanced, near continuum regime, and (3) the potential-enhanced near free molecular regime. Simple closed-form expressions for evaluating the collision kernel are given for the former two regimes.

II. THEORETICAL FRAMEWORK FOR TRANSITION REGIME COLLISIONS

A. Dimensional Analysis

In the continuum (hydrodynamic) limit, the collision kernel, β_{ij}, for hard-sphere collisions between two entities i and j is expressed as[21]:

$$\beta_{ij} = 4\pi \frac{kT}{f_{ij}} \left(a_i + a_j\right) \tag{2a}$$

where k is Boltzmann's constant, T is system temperature, a_i and a_j are the radii of entities i and j, respectively, and f_{ij} is the reduced friction factor[19], i.e. $f_{ij} = f_i f_j/(f_i+f_j)$ (where f_i and f_j are the friction factors of entities i and j, respectively). Conversely, in the free molecular (collisionless) limit, the collision kernel for hard-sphere entities is expressed as[57]:

$$\beta_{ij} = \left(\frac{8\pi kT}{m_{ij}}\right)^{1/2} \left(a_i + a_j\right)^2 \tag{2b}$$

where m_{ij} is the reduced mass, defined as $m_{ij} = m_i m_j/(m_i+m_j)$ where m_i and m_j are the masses of entities i and j, respectively. From equations (2a) and (2b) it is clear that β_{ij} depends upon kT, a_i+a_j, f_{ij}, and m_{ij}. Standard dimensional analysis of the non-repeating variables β_{ij} and kT (the energy which drives collisions) gives the dimensionless collision kernel, H as[19, 56]:

$$H = \frac{\beta_{ij} m_{ij}}{f_{ij}\left(a_i + a_j\right)^3} \tag{3a}$$

and the diffusive Knudsen number, $\mathrm{Kn_D}$ (ratio of the collision persistence distance, which scales with $[kTm_{ij})^{1/2}/f_{ij}$, to the collision length scale)[18, 58-59], as:

$$\mathrm{Kn_D} = \frac{\left(kTm_{ij}\right)^{1/2}}{f_{ij}\left(a_i + a_j\right)} \tag{3b}$$

$\mathrm{Kn_D}$, also referred to previously as a dimensionless system temperature[60], governs mass transfer processes in the transition regime (such as collisions), and is distinct from traditional Knudsen number[61] (the ratio of the hard sphere mean free path of gas molecules to an appropriate length scale for a particle), which governs transition regime momentum transfer from gas molecules to suspended entities. The relationship $H(\mathrm{Kn_D})$ thus describes the collision kernel in the transition regime. In the continuum ($\mathrm{Kn_D} \rightarrow 0$) and free molecular limits ($\mathrm{Kn_D} \rightarrow \infty$), $H(\mathrm{Kn_D})$ takes the functional forms given in equations (4a) and (4b), respectively:

$$H = 4\pi \mathrm{Kn_D^2} \qquad \text{as} \qquad \mathrm{Kn_D} \rightarrow 0 \tag{4a}$$

$$H = \left(8\pi\right)^{1/2} \mathrm{Kn_D} \qquad \text{as} \qquad \mathrm{Kn_D} \rightarrow \infty \tag{4b}$$

In the transition regime, a number of methods[18-20, 28, 31, 33, 56, 62], including the flux-matching approach, lead to prediction of the $H(\mathrm{Kn_D})$ relationship, with all $H(\mathrm{Kn_D})$ predictions within 5% of one another across the entire $\mathrm{Kn_D}$ range. For example, from prior Langevin equation-based mean first passage time calculations[19, 56], $H(\mathrm{Kn_D})$ is given as:

$$H = \frac{4\pi \mathrm{Kn_D^2} + C_1 \mathrm{Kn_D^3} + \left(8\pi\right)^{1/2} C_2 \mathrm{Kn_D^4}}{1 + C_3 \mathrm{Kn_D} + C_4 \mathrm{Kn_D^2} + C_2 \mathrm{Kn_D^3}} \tag{5}$$

where C_1 =25.836, C_2 = 11.211, C_3 = 3.502, and C_4 = 7.211.

We now consider collisions in the presence of both thermal energy and Coulombic potential energy, and similarly attempt to develop appropriate independent and dependent dimensionless ratios to describe the collision kernel in the transition regime under such

conditions. In the continuum limit, the collision kernel in presence of potential interactions is expressed as:

$$\beta_{ij} = 4\pi \frac{kT}{f_{ij}} \left(a_i + a_j\right) \eta_c \tag{6a}$$

where η_c is the continuum limit enhancement factor, which, for the Coulombic potential, is expressed as[21]:

$$\eta_c = \frac{\psi_E}{1 - \exp\left(-\psi_E\right)} \tag{6b}$$

Similarly, in the free molecular limit, the collision kernel, when modified to account for potential energy, is expressed as:

$$\beta_{ij} = \left(\frac{8\pi kT}{m_{ij}}\right)^{1/2} \left(a_i + a_j\right)^2 \eta_{FM} \tag{6c}$$

where the free molecular limit enhancement factor, η_{FM}, is given as[25]:

$$\eta_{FM} = 1 + \psi_E \tag{6d}$$

for attractive Coulombic interactions and as[63]:

$$\eta_{FM} = \exp\left(\psi_E\right) \tag{6e}$$

for repulsive Coulombic interactions. The potential energy to thermal energy ratio for the Coulombic potential, Ψ_E, is expressed as:

$$\psi_E = \frac{-z_i z_j e^2}{4\pi\varepsilon_0 \left(a_i + a_j\right) kT} \tag{6f}$$

where z_i and z_j are the integer charge levels of entities i and j, respectively, ε_0 is the permittivity of the background gas, and e is the unit charge. As Ψ_E is positive for collisions between

attracting entities and negative for collisions between repelling entities, η_c and η_{FM} are greater than 1.0 for attractive collisions, and less than 1.0 for repulsive collisions.

Unlike the collision kernel in the presence of thermal energy alone, nondimensionalization of the collision kernel in the presence of both thermal and potential energy requires that the dimensionless collision kernel be expressed as a function of two independent dimensionless variables. The first of the independent variables is Ψ_E. To arrive at the remaining dimensionless ratios (H and Kn_D), we require that dimensionally, equations (6a) and (6c) hold valid in their corresponding limits, and dimensionlessly, as $\mathrm{Kn_D}\rightarrow 0$ and $\mathrm{Kn_D}\rightarrow\infty$, equations (4a) and (4b), respectively, hold valid. These conditions lead to H expressed by the equation:

$$H = \frac{\beta_{ij} m_{ij} \eta_C}{f_{ij}\left(a_i + a_j\right)^3 \eta_{FM}^2} \tag{8a}$$

and $\mathrm{Kn_D}$ expressed by the equation:

$$\mathrm{Kn_D} = \frac{\left(kTm_{ij}\right)^{1/2} \eta_C}{f_{ij}\left(a_i + a_j\right)\eta_{FM}} \tag{8b}$$

B. Mean First Passage Time Calculations

With the above dimensional analysis, the challenge becomes the inference of H at specified values of $\mathrm{Kn_D}$ and Ψ_E, which is accomplished here via mean first passage time calculations. Related calculations have been used previously not only to examine gas-phase collisions[19, 36, 56], but also in the continuum limit to examine macromolecular reaction rates[22, 64-65] and, using the Hubbard-Douglas approximation, the continuum regime friction factor for arbitrarily shaped bodies[65-67]. For the calculations performed here we assume that the relative

motion between the colliding entities can be described by monitoring the trajectory of a point mass with mass m_{ij} and friction factor f_{ij} within a simulation domain of prescribed dimensions until it collides with a stationary spherical entity of radius a_i+a_j. Motion of the point mass within the domain is described by a Langevin equation[36], i.e. a force balance accounting for the drag (viscous) force, stochastic diffusion force, and the electrostatic force between the two entities. In utilizing a single Langevin equation for this calculation, two assumptions must hold valid (in addition to the assumed negligible mass of the background gas). First, the ratios $\theta_m = m_i/(m_i+m_j)$ and $\theta_f = f_i/(f_i+f_j)$ must be equivalent, as is the case for two equal sized particles of the same material, or for an ion-particle collision wherein the particle is significantly larger and more massive than the ion. Between these two limiting cases, for spherical particles of similar density, θ_m and θ_f are in close proximity, to the point where the errors brought about by their assumed equality are small[19]. Second, in all Langevin equation based approaches, it is assumed that the process under examination occurs on a time scale for which the drag force and stochastic diffusive force, which both arise from collisions with the bath gas molecules, may be treated as distinguishable quantities. This assumption is also reasonable for entities in dilute gas-phase systems. Dimensionally, the Langevin equation for the point mass is written as:

$$m_{ij}\frac{d\vec{v}}{dt} = -f_{ij}\vec{v} + \vec{F}_{Coul} + \vec{\mathrm{M}}(t) \qquad (9a)$$

where $\vec{v}$ is the relative velocity between the two colliding entities (the velocity of the point mass), t is time, $\vec{F}_{Coul}$ is the Coulombic force vector between colliding entities, and $\vec{\mathrm{M}}(t)$ is the diffusive force vector for a point mass with mass m_{ij} and friction factor f_{ij}, with equal magnitude in all principal directions[19]. With $\vec{x}$ as the position vector of the point mass, and with

$\vec{v}^* = \dfrac{m_{ij}\vec{v}}{f_{ij}(a_i + a_j)}$ as well as $\vec{x}^* = \dfrac{\vec{x}}{(a_i + a_j)}$, the solution of the Langevin equation for the point mass can be written dimensionlessly as[68]:

$$\vec{v}^*(\tau + \Delta\tau) = \vec{v}^*(\tau)\exp(-\Delta\tau) - \psi_E \mathrm{Kn}_\mathrm{D}^2 \frac{\eta_{FM}^2}{\eta_C^2}(1 - \exp(-\Delta\tau))\frac{\hat{r}}{r^{*2}} + \vec{A}_1 \tag{9b}$$

$$\vec{x}^*(\tau + \Delta\tau) = \vec{x}^*(\tau) + \left(\vec{v}^*(\tau + \Delta\tau) + \vec{v}^*(\tau) + 2\psi_E \mathrm{Kn}_\mathrm{D}^2 \frac{\eta_{FM}^2}{\eta_C^2}\frac{\hat{r}}{r^{*2}}\right)\left(\frac{1 - \exp(-\Delta\tau)}{1 + \exp(-\Delta\tau)}\right) - \psi_E \mathrm{Kn}_\mathrm{D}^2 \frac{\eta_{FM}^2}{\eta_C^2}\frac{\hat{r}}{r^{*2}} + \vec{A}_2 \tag{9c}$$

where τ is the nondimensionalized time *(*$\tau = (f_{ij}/m_{ij})t$*)* and $\Delta\tau$ is small change in τ, thus $\vec{v}^*(\tau + \Delta\tau)$, $\vec{x}^*(\tau + \Delta\tau)$, $\vec{v}^*(\tau)$, and $\vec{x}^*(\tau)$ denote the point mass dimensionless velocities and positions at dimensionless times τ and $\tau + \Delta\tau$, respectively. The vector $\hat{r}$ and the scalar r^* denote a unit vector in radial direction and the dimensionless distance of the point mass from the origin in the simulation domain, respectively. Finally, $\vec{A}_1$ and $\vec{A}_2$ are both Gaussian distributed random vectors with zero mean and variances given in equations (9d) and (9e), respectively:

$$\left\langle \vec{A}_1^{\,2} \right\rangle = 3\mathrm{Kn}_\mathrm{D}^2 \frac{\eta_{FM}^2}{\eta_C^2}(1 - \exp(-2\Delta\tau)) \tag{9d}$$

$$\left\langle \vec{A}_2^{\,2} \right\rangle = 6\mathrm{Kn}_\mathrm{D}^2 \frac{\eta_{FM}^2}{\eta_C^2}\left(\Delta\tau - 2\left(\frac{1 - \exp(-\Delta\tau)}{1 + \exp(-\Delta\tau)}\right)\right) \tag{9e}$$

A cubical simulation domain is used with periodic boundary conditions employed on the domain surface. Calculations are performed with prescribed Kn_D, Ψ_E, $\Delta\tau$, and dimensionless box side length, s (all dimensions are normalized by $a_i + a_j$), with no other inputs required. At the start of each calculation, the point mass is placed at a random location on the box surface, with a velocity sampled from equation (9d), while the stationary particle is placed in the center of the

domain. The motion of the point mass is monitored with equations (9b-9e) until it collides with the fixed central sphere, at which point the dimensionless time required for collision τ_i is recorded, a new point mass is placed on the domain surface, and calculation of the collision time is again repeated. After N collisions have been monitored, the mean first passage time, τ_{mean} is calculated as:

$$\tau_{mean} = \frac{\sum_{i=1}^{N} \tau_i}{N} \tag{10}$$

For each set of $\mathrm{Kn_D}$, Ψ_E, $\Delta\tau$, and s values, a value of N in the range 500-1500 is chosen, such that the relative standard deviation of τ_{mean} is less than 1% over the most recent 200 collisions. The dimensionless collision kernel is subsequently determined from τ_{mean} as:

$$H = \frac{s^3 \eta_C}{\tau_{mean} \eta_{FM}^2} \tag{11}$$

Equation (11) follows directly from the definition of H in equation (8a), as well as the definitions of the dimensionless parameters s and τ_{mean}. Although $\Delta\tau$ and s are inputs for each calculation, we are interested in results where the mean first passage time is insensitive to both $\Delta\tau$ and s, i.e. as $\Delta\tau \to 0$ and $s \to \infty$. The criteria $\Delta\tau = 0.005 \mathrm{Kn_D}^{-2}$ when $|\psi_E| < 1$ and $\Delta\tau = 0.005 \mathrm{Kn_D}^{-2} \Psi_E^{-1}$ when $|\psi_E| \geq 1$ are found satisfactory to mitigate the influence of timestep on calculation results. To mitigate the effects of domain size, dimensionless side lengths ranging from 50-200 are used, increasing with increasing Ψ_E such that at the domain surface, the influence of the electrostatic force on the change in point mass velocity and position is substantially less than the influence of diffusion ($\vec{A}_2$ and $\vec{A}_1$) for the prescribed $\Delta\tau$. While the aforementioned values are found appropriate for mean first passage time calculations, smaller timesteps and larger domain side

lengths are also used to ensure that results are insensitive to both these values, and to further ensure convergence, calculations of H for a given Kn_D and Ψ_E are repeated 10 times, with reported values as the average of these 10 calculations. H values are thus determined for attractive collisions with Ψ_E = 0.01 to 30 (at 300 K this corresponds to singly charged particles with a_i+a_j ranging from 5.56 μm down to 1.85 nm) and for repulsive collisions with Ψ_E = -0.01 to -3. Finally, as extremely small timesteps are required to probe situations of large Kn_D and Ψ_E, computations are limited to Kn_D values below 30 for most Ψ_E.

The inferred H values apply for entities which are sufficiently dilute such that the time for collision is much less than the mixing time for the system, and concentration gradients do not develop as a result of collisions. While this condition is in conflict with the original theory of Smoluchowski in the analysis of thermally driven collisions[23], Veshchunov[31, 69] has recently shown that the dilute limit assumption leads to similar results as does the Smoluchowski approach, at least in the case of hard sphere collisions in three dimensions. Described in the results and discussion section, by the convergence of mean first passage time inferred collision kernels to the appropriate continuum and free molecular limits, we show that this holds true in the presence of potential interactions between colliding entities as well.

III. MEAN FIRST PASSAGE TIME RESULTS AND INTERPRETATION

A. Influence of Kn_D *and* Ψ_E

Attractive potential calculation results are shown as functions of Kn_D for $0.01 \leq \Psi_E \leq 0.5$ in figure 1a and for $0.7 \leq \Psi_E \leq 30$ in figure 1b, respectively. Results are represented in terms of the percent deviation between the calculation and the expected $H(Kn_D)$ for hard sphere collisions (equation 5) in figure 1a, while in figure 1b $H(Kn_D)$ curves at fixed Ψ_E are shown directly. For

further comparison, also shown in both figures are the continuum and free molecular limiting curves (equations 4a and 4b), the $H(\mathrm{Kn_D}, \Psi_E)$ taken from the flux matching theory put forth by D'yachkov et al[52], which, when the Coulomb potential is considered, only differs from the predictions of Fuchs's original theory[1] by several percent across the entire $\mathrm{Kn_D}$ range, and is expressed as:

$$H = 4\pi \mathrm{Kn}_\mathrm{D}^2 \left(F\left(\mathrm{Kn}_\mathrm{D}, \psi_E\right)\right)^{-1} \tag{12a}$$

$$F\left(\mathrm{Kn}_\mathrm{D}, \psi_E\right) = \frac{(2\pi)^{1/2}\,\mathrm{Kn}_\mathrm{D}\eta_{FM}\exp\left(\dfrac{-\psi_E}{1+\dfrac{\eta_{FM}}{\eta_C}\mathrm{Kn}_\mathrm{D}}\right)}{\left(1+\dfrac{\eta_{FM}}{\eta_C}\mathrm{Kn}_\mathrm{D}\right)^2 - \dfrac{\eta_{FM}}{\eta_C}\mathrm{Kn}_\mathrm{D}\left(2+\dfrac{\eta_{FM}}{\eta_C}\mathrm{Kn}_\mathrm{D}\right)\exp\left(\dfrac{-\psi_E}{\left(1+\dfrac{\eta_{FM}}{\eta_C}\mathrm{Kn}_\mathrm{D}\right)\left(2+\dfrac{\eta_{FM}}{\eta_C}\mathrm{Kn}_\mathrm{D}\right)}\right)} + \frac{1-\exp\left(\dfrac{-\psi_E}{1+\dfrac{\eta_{FM}}{\eta_C}\mathrm{Kn}_\mathrm{D}}\right)}{1-\exp\left(-\psi_E\right)} \tag{12b}$$

and finally the proposed equation of Gatti and Kortshagen[53], expressed as:

$$H = 4\pi \mathrm{Kn}_\mathrm{D}^2\left(1-\left(1+\frac{\pi^{1/2}\alpha\eta_C\psi_E}{2\eta_{FM}\mathrm{Kn}_\mathrm{D}}\right)\exp\left(\frac{-\pi^{1/2}\alpha\eta_C\psi_E}{2\eta_{FM}\mathrm{Kn}_\mathrm{D}}\right)\right) + (8\pi)^{1/2}\,\mathrm{Kn}_\mathrm{D}\left(1+\frac{2\pi^{1/2}\alpha^3\psi_E^3\eta_C}{9\eta_{FM}\mathrm{Kn}_\mathrm{D}}\right)\exp\left(\frac{-\pi^{1/2}\alpha\eta_C\psi_E}{2\eta_{FM}\mathrm{Kn}_\mathrm{D}}\right) \tag{13}$$

In equations (12) and (13), η_{FM} and η_C are defined in equations (6b) and (6d), respectively, and α = 1.22. Although equation (13) is adapted from Gatti and Kortshagen, it has been reformulated following their approach such that as $\mathrm{Kn_D}\rightarrow 0$, the expression approaches the expected value of $4\pi\mathrm{Kn_D}^2$; in the original work the influence of thermal energy on the collision process in the continuum regime was neglected. As noted in the introduction section, the Gatti

and Kortshagen proposed $H(\mathrm{Kn_D}, \Psi_E)$ curve results from the assumption that the collision rate can be calculated as a linear combination of the collision rate for entities moving via continuum transport, the collision rate for entities moving via free molecular transport, and the collision rate for entities where a single gas molecule collision occurs prior to the charged entity collision. For this reason we henceforth refer to the Gatti and Kortshagen proposed curve as linear combination theory, while referring to the curve from D'yachkov et al as flux matching theory.

Focusing first on $H(\mathrm{Kn_D})$ curves for $\Psi_E \leq 0.5$, with the exception of calculations at high $\mathrm{Kn_D}$ (5-10) with $\Psi_E = 0.5$, all calculated H values are within 6% of the expected $H(\mathrm{Kn_D})$ values determined for hard spheres. Variations of +/- 6% are well within the bounds of expected statistical variation for mean first passage time calculations[19], and we thus conclude that for attractive Coulombic potentials with $\Psi_E \leq 0.5$, $H(\mathrm{Kn_D})$ may be calculated using equation (5), with the definitions of H and $\mathrm{Kn_D}$ adjusted (equations (8a) and (8b)) for convergence to the correct low $\mathrm{Kn_D}$ and high $\mathrm{Kn_D}$ limiting expressions. Flux matching theory predictions of $H(\mathrm{Kn_D})$ are also within +/- 6% of both the hard sphere curve and calculated values, in line with prior comparisons made to limiting sphere theory in this Ψ_E range[3-4, 46, 49]. Conversely, even with the aforementioned corrections made, the $H(\mathrm{Kn_D}, \Psi_E)$ curve from linear combination theory is in sharp contrast with our calculations and limiting sphere predictions, suggesting it is not appropriate for collision rate calculations in these circumstances.

For Ψ_E in the 0.7 to 30 range, clear deviations of $H(\mathrm{Kn_D})$ from the hard sphere curve are evident. As Ψ_E increases, the $\mathrm{Kn_D}$ value at which $H(\mathrm{Kn_D})$ departs from the continuum curve also increases greatly. For example, the continuum limit H value ($4\pi\mathrm{Kn_D}^2$) at $\mathrm{Kn_D} = 2$ is 5.5 times larger than the calculated $H(\mathrm{Kn_D})$ at $\Psi_E = 0$, while for $\Psi_E = 30$ at this $\mathrm{Kn_D}$ the continuum limit prediction differs from the calculated value by less than 5%. Similarly, the $\mathrm{Kn_D}$ value at which

$H(\mathrm{Kn_D})$ approaches the free molecular limit also increases drastically with Ψ_E, with differences between the free molecular curve and $H(\mathrm{Kn_D})$ persisting beyond $\mathrm{Kn_D} = 30$ at $\Psi_E = 1$. These two influences combined lead to a shift in the $\mathrm{Kn_D}$ range corresponding to the transition regime (where neither limiting expression applies). Along with this shift, unlike the hard sphere curve, in the presence of potential energy $H(\mathrm{Kn_D})$ is not bounded below both the predicted continuum and free molecular limits; a collision rate faster the free molecular limit prediction is achievable. The shift in the transition regime $\mathrm{Kn_D}$ range with increasing Ψ_E is expected from both flux matching and linear combination theories. Neither of these approaches, however, appears to correctly predict the dimensionless collision kernel in the transition regime. Flux matching theory consistently underestimates the collision kernel outside the continuum regime at large Ψ_E, in line with conclusions of comparisons of flux matching predictions to experimental examined collision rates in the Ψ_E = 2-4 range[53]. The agreement between mean first passage time calculations and linear combination theory improves in the $\Psi_E > 0.7$ range and is quite reasonable for $\Psi_E = 1-3$, the range for which it was originally developed. Nonetheless, linear combination theory leads to a consistent overestimation of $H(\mathrm{Kn_D})$ in the transition regime across all Ψ_E.

Possible origins of the discrepancies between mean first passage time calculation results, flux matching theory, and other approaches to determine the collision kernel are discussed in detail in the subsequent section. Prior to this discussion, however, we report results of mean first passage time calculations for collisions in the presence of repulsive potentials. Figure 2 shows $H(\mathrm{Kn_D})$ calculated in the presence of repulsive Coulombic energy, with Ψ_E = -0.03 to -3, along with the continuum and free molecular limiting expressions, the hard sphere curve, and the

predictions of D'yachkov et al[52] for collisions between repelling entities, for which $H(\mathrm{Kn}_D, \Psi_E)$ is expressed as:

$$H = 4\pi \mathrm{Kn}_\mathrm{D}^2 \left(G\left(\mathrm{Kn}_\mathrm{D}, \psi_E\right)\right)^{-1} \tag{14a}$$

$$G\left(\mathrm{Kn}_\mathrm{D}, \psi_E\right) = \frac{\exp\left(\dfrac{\psi_E}{1+\dfrac{\eta_{FM}}{\eta_C}\mathrm{Kn}_\mathrm{D}}\right) - 1}{\exp\left(\psi_E\right) - 1} + \left(2\pi\right)^{1/2}\mathrm{Kn}_\mathrm{D} \tag{14b}$$

Contrary to results with attractive potentials, all calculated collision kernels for repulsive potentials remain close (most results within 12%) to the hard sphere curve, even at $\left|\psi_E\right| \geq 1$. Further, irrespective of Ψ_E, for repulsive Coulombic potentials, equation (14) is within 5% of the hard sphere curve across the entire Kn_D range. The convergence of mean first passage time calculations and flux matching theory predictions in this instance suggests that for repulsive potentials, equation (5), equation (14), or equivalently, any collision kernel expression derived for hard spheres[19, 31] with correctly modified definitions of the dimensionless collision kernel and diffusive Knudsen number can be used reliably to predict collision rates in the presence of repulsive potentials.

B. Limitations of Flux Matching Theory

It is clear from mean first passage time calculations that although flux match theory appears to correctly predict the collision kernel for repulsive potentials as well as attractive potentials with low values of Ψ_E, both flux matching and linear combination theory fail to predict the collision kernel in the transition regime at large positive Ψ_E. While prior work does indeed suggest that flux matching theory may fail under these circumstances[44], we believe the

calculations performed here provide the most direct evidence to-date that application of flux matching theory to large Ψ_E situations is problematic.

We thus compare flux matching theory to mean first passage time calculations in terms of the process by which calculations are carried out in each approach. In both, the collision rate/kernel is inferred via examination of the collision of a point mass with an absorbing sphere. In all incarnations of flux matching theory[1, 24, 41-42, 51-52], the flow rate/current of point masses to the surface of a limiting sphere, which has a dimensionless radius[24, 29-30] of approximately $1+(\eta_{FM}/\eta_C)\mathrm{Kn_D}$ and surrounds an immobile sphere of unit radius, is first calculated. The point masses move to the limiting sphere via continuum transport; thus, a modified form of Fick's law is used in evaluating the point mass flow rate[20]. The fraction of point masses that enter the limiting sphere and subsequently collide with the central sphere is next calculated. This ultimately enables the collision kernel calculation as the product of the point mass flow rate and the fraction of point masses that collide with the central sphere, divided by the number concentration of point masses. In determining the fraction of point masses which collide with the central sphere, free molecular trajectory calculations are typically carried out, and to initialize these calculations, the point masses are assumed to have either the mean thermal speed[1] or follow a Maxwell-Boltzmann distribution[52]. On the contrary, with large Ψ_E, point masses are exposed to a strong attractive force, and flux matching theory may fail if the resulting increase in speed beyond the mean thermal speed is not correctly accounted for. Mean first passage time calculations do account for this change in speed by construction, and Figure 3 shows the average point mass speed (dimensionless) as a function of dimensionless radial coordinate in the calculation domain for selected $\mathrm{Kn_D}$ and Ψ_E, from our calculations. In the dimensionless system employed, the dimensionless mean thermal speed, v_{th}^*, is given as:

$$v_{th}^{*} = \left(\frac{8}{\pi}\right)^{1/2} \frac{\eta_{FM}}{\eta_C} \mathrm{Kn}_\mathrm{D} \tag{15}$$

Therefore, in Figure 3, a value of 1.0 denotes that the point mass mean speed is equal to the mean thermal speed. Also noted on the graphs in Figure 3 are the approximate limiting sphere radii for each Kn_D (which varies slightly with Ψ_E). As expected for $\Psi_E = 0$, at all Kn_D, the average speed of the point mass in calculations is equal to the mean thermal speed. This also appears to hold approximately true for $\Psi_E = \pm 1$. However, for $\Psi_E = 3, 10,$ and 30 with $\mathrm{Kn}_\mathrm{D} \geq 0.1$, as the point mass approaches the central sphere, the average speed of the point mass increases. Larger increases in speed are evident at higher Kn_D, such that the point mass speed can be several multiples of the mean thermal speed close to the sphere surface. In addition, for these high Ψ_E cases, at the surface of a constructed limiting sphere (with dimensionless radial coordinates noted by dashed gray vertical lines in each graph), the point mass speed is larger than the thermal speed, with the maximum speed increase at the limiting sphere surface found for $\mathrm{Kn}_\mathrm{D} = 1$.

Coupled with an initial speed distribution in flux matching theory calculations is the initial distribution of point masses on the limiting sphere surface, i.e. the distribution of point mass impact parameters[1, 70]. At any point in space, the ratio of the impact parameter for a point mass to its radial coordinate, b/r, can be calculated as the sine of the angle formed between the point masses velocity vector and position vector. For uniformly distributed impact parameters, which would be expected in the absence of potential interactions and which are assumed on the limiting sphere surface in flux matching theory, the average value of b/r, $(b/r)_{ave}$, is $\pi/4$ (0.7854). However, associated with the change in speed, at high Ψ_E, $(b/r)_{ave}$ is expected to decrease, with the direction of the point mass velocity vectors biased towards the center of the collecting sphere.

As with changes in speed, the change in impact factor distribution due to potential energy is accounted for in mean first passage time calculations, with $(b/r)_{ave}$ as a function of the dimensionless radial position in calculations displayed in Figure 4. Under most conditions, $(b/r)_{ave}$ fluctuates about its expected hard sphere value, with the fluctuations attributable to the statistical nature of mean first passage time calculations. However, at intermediate Kn_D (*0.1-1.0*) and large Ψ_E, a decrease in $(b/r)_{ave}$ is indeed evident, further demonstrating that flux matching theory makes use of inappropriate boundary conditions on the constructed limiting sphere surface.

Although certain (Kn_D, Ψ_E) pairs are readily found for which flux matching theory fails to account for the correct speed and impact parameter distributions on the limiting sphere surface, it nonetheless gives rise to a near identical collision kernel to mean first passage time calculations under many of these conditions. For example, at $Kn_D = 1$ and $\Psi_E = 10$, where the point mass speed is well above the mean thermal speed and the impact parameter distribution is skewed towards the collecting sphere center, the collision kernels predicted by both approaches differ by only 5%. In such instances, it is readily observed that (1) the predicted collision kernel is in good agreement with continuum predictions, and (2) in flux matching theory calculations all point masses entering the limiting sphere are collected, hence little to no error is introduced by the incorrect boundary conditions. It thus appears that it is only for sufficiently high Kn_D (outside the continuum regime) and high Ψ_E (e.g. $\Psi_E = 30$) where the inappropriate boundary conditions have consequences in collision kernel calculation. Conversely, there are a number of (Kn_D, Ψ_E) pairs for which the mean first passage time determined point mass speeds and impact parameters are near identical to expected values for hard spheres, and yet flux matching theory predicts a much lower collision kernel value than is found in mean first passage time calculations

(e.g. 61.4% different at $Kn_D = 10$, $\Psi_E = 3$). While not evident from speed or impact parameter calculations, the low collision kernel values in these instances, which are for $\Psi_E \geq 0.5$ and outside the continuum limit, arise because of the failure of flux matching theory to account for point mass-gas molecule collisions occurring close to the collecting sphere surface and inducing collision with the central sphere. Such collisions may result in a reduced speed for the charge carrying point mass, such that the point mass can be captured by the central collecting sphere. This type of occurrence, termed three-body trapping[42] or a charge-exchange collision[53], can become the dominant mechanism by which collisions occur at high Kn_D and Ψ_E. By use of the Langevin equation to describe point mass motion, three body trapping is considered in mean first passage time calculations. It is also accounted for in linear combination theory; however, based on mean first passage time results (and our presumption that these calculations correctly lead to determination of the collision kernel to +/-5%), it appears that outside the $\Psi_E = 0.1 - 2.0$ range the increase in collision rate due to three body trapping is overestimated with this approach. Aware that three body trapping is not considered in the original derivation of flux matching theory, Hoppel and Frick[42] attempted to modify Fuchs's approach specifically for particle-ion collisions by noting that a calculation of the collision rate between a particle and a point mass ion for positive Ψ_E should converge to the positive ion-negative ion recombination rate when the particle is of similar size to the ions themselves. Requiring an experimentally-determined ion recombination rate as an input, they incorporated Natanson's method[71] to determine the rate of three body trapping based collisions into Fuchs's original approach. While this model perhaps allows for more reasonable approximation of the collision kernel than the original flux matching theory, there are several possible issues with utilizing Hoppel and Frick's approach. First, it requires a "tuning constant" input from experiments and is therefore not a complete theory for

describing collisions. Second, while the ion recombination rate may be inferred from experiments correctly, collisions between two ions may be subject to different potentials than the ion-particle potential, and further the molecular structures of ions may have a strong influence on the collision rate between oppositely charged ions (i.e. while modeling particles as spheres be may acceptable, it is often inaccurate to model ions as spheres in ion-ion collisions)[72-74]. When the influences of ion structure and the ion-ion potential interaction are considered, there is no reason to expect that the particle-ion collision kernel function should collapse to the ion-ion collision kernel at large Kn_D. Finally, as is customary in flux matching theory, Hoppel and Frick's approach does not address the issues of incorrect speed and impact parameter distributions, which become important in conjunction with three body trapping.

C. Coulombic Capture Radii

Overall, based on mean first passage time calculations, we find that neither any existing incarnation of flux matching theory nor linear combination theory satisfactorily describes collisions in the gas phase in the presence of attractive Coulombic energy across a wide range of Kn_D and Ψ_E. Moreover, in the instances where flux matching theory does agree with calculations, the hard sphere inferred $H(Kn_D)$ expression with adjusted definitions of H and Kn_D for the Coulombic potential is also in excellent agreement with calculations. We therefore propose that the modified hard sphere $H(Kn_D)$ curve be used for collision kernel calculation under these conditions, and additionally now attempt to use mean first passage time results to fit an appropriate functional form for $H(Kn_D, \Psi_E)$ in the $\Psi_E \geq 0.5$ range.

Although our results are typically in poor agreement with linear combination theory predictions, there are some important features to this theory which can be used in the analysis of

mean first passage time calculations. Central to linear combination theory development is the definition of a capture radius, i.e. the radial distance at with the thermal energy is equal to the potential energy, such that for a monotonic attractive potential, a point mass is highly likely to collide with the absorbing sphere upon arriving at the capture radius. For the Coulomb potential, the capture radius, R_C, is defined as:

$$R_C = \max\left[a_i + a_j, \frac{2}{3}\psi_E \left(a_i + a_j\right) \right] \tag{16}$$

and with $\Psi_E > 1.5$, the capture radius is larger than the absorbing sphere radius. The influence of a capture radius at high Ψ_E can be observed in mean first passage time calculations. Figure 5 shows the probability, *P(r*),* that a point mass at a given dimensionless radial distance from the domain origin will collide with the central absorbing sphere for selected Kn_D and Ψ_E. Calculation for these curves proceeds as follows: for each value of r^*, it is determined whether a point mass, having reached a dimensionless distance r^* from the domain center, will collide with the central sphere rather than return to the domain boundary. If the point mass reaches the absorbing sphere, then a *collision* is counted for all r^* up to *s*, as point masses are initiated at least a distance *s* from the domain center. However, if a point mass returns to the domain surface, a *miss* is counted for all values of r^* ranging from *s* down to the minimum r^* value the point mass reached. $P(r^*)$ is then calculated as *collisions / (misses + collisions)* for each r^*. While this calculation approach leads to inaccuracies (underestimation) for r^* close to *s*, $P(r^*)$ near *s* is close to zero and otherwise the probability that a point mass will collide with the central sphere is accurately determined for all other r^*. For $\Psi_E < 1.5$ and including repulsive potentials, *P(r*)* curves are similar to one another, with little shift in *P(r*)* curves even when comparing those with positive and negative Ψ_E. Conversely, for the examined cases with $\Psi_E = 3$, *10*, and

30 at all examined Kn_D, *P(r*)* curves are clearly shifted, such that at the dimensionless capture radius ($2\Psi_E/3$), probability of collision is typically ≥0.80.

Gatti and Kortshagen[53] show that when the Knudsen number is defined using the capture radius as the normalizing length scale in lieu of the sum of colliding entity radii, the shift in Knudsen number range for which the collision kernel approaches its expected continuum value is not apparent, implying that the collision radius is the correct normalizing length for the Knudsen number. Lushnikov and Kumala[41] also propose that the Knudsen number for charged entity collisions at large Ψ_E should be defined based upon Coulombic length scale, as opposed to colliding entity radii. Moreover, the physics of the collision process suggests that an appropriately defined capture radius is the correct normalizing length scale for collisions in the presence of potential energy; at the surface of the collision radius, the capture probability is close to 1.0, and similarly the probability of avoiding collision is close to 0. Therefore, if transport to the capture radius surface (at which point collision occurs) can be described solely as a continuum regime process, then it follows that the entire collision process can be described by continuum transport relations. Only under circumstances where colliding entities can move in close proximity to one another on time scales where (1) motion is not described by continuum transport and (2) a collision can be avoided, will the collision kernel deviate from the expected continuum value. Given these arguments and the suggestions of prior work, we define the potential Knudsen number, Kn_Ψ as:

$$\mathrm{Kn}_\psi = \frac{3\left(kTm_{ij}\right)^{1/2}\eta_C}{2f_{ij}\psi_E\left(a_i + a_j\right)\eta_{FM}} = \frac{3\mathrm{Kn}_\mathrm{D}}{2\psi_E} \tag{17}$$

and also propose that the governing parameter for collisions in the presence of thermal and Coulombic energy will be the minimum of Kn_D and Kn_Ψ. Considering all calculations for which

$\Psi_E \geq 0.5$, the ratio of inferred H to the expected continuum limit value, i.e. $H/4\pi Kn_D^2$, is plotted as a function of the minimum of Kn_D, Kn_Ψ in Figure 6. Across the entire examined Ψ_E range, these results collapse remarkably well to a single curve, giving further credence to the concept of a capture radius for attractive collisions.

Also plotted as a dashed line in Figure 6 is the function:

$$\frac{H}{4\pi Kn_D^2} = \frac{1}{1 + B_1\left(\min\left[Kn_D, Kn_\psi\right]\right)^{B_2}} \tag{18}$$

where $B_1 = 1.598$ and $B_2 = 1.1709$, which are determined via fitting calculation results. For scenarios for which $\min[Kn_D, Kn_\Psi] \leq 2.5$, equation (18) better agrees with calculation results than does a modification to the hard sphere $H(Kn_D)$ curve, with equation (18) predictions within +/- 10% of most calculated points. We thus propose that when $\Psi_E \geq 0.5$, equation (18) can predict the dimensionless collision kernel in the near-continuum regime with reasonable accuracy. We note, however, equation (18) does not converge to the correct free molecular limiting result, and even with the definition of Kn_Ψ, we are not able find a collapsed function which can predict the collision kernel in the near free molecular regime with any degree of accuracy. Fortunately, considering charged entities, high Kn_D is correlated with high Ψ_E, in the majority of aerosol systems and a number of dusty plasma systems. Therefore, most high Ψ_E collisions occur with a Kn_Ψ associated with the near continuum collision regime (with the exception of highly charged, supermicrometer particles in a low pressure environment).

D. Collision Kernel Calculation for Population Balance Models

Often, the underlying purpose of calculating collision kernels is for their use in particle/plasma grain population balance models, i.e. systems of ordinary or partial differential

equations used to monitor the changes in number concentrations of particles of a given size and charge state over space and time dimensions[11, 15, 75-76]. For this reason, we develop a "phase space diagram" which denotes the appropriate collision kernel expression for use in charged entity collision rate calculations at a given Kn_D and Kn_Ψ (Figure 7). In the phase space diagram, Kn_Ψ and Kn_D are plotted on the principal axes in the range where Ψ_E is positive. The line $Kn_D = Kn_\Psi/3$ is noted, which corresponds to $\Psi_E = 0.5$ and below which are (Kn_D, Kn_Ψ) pairs where the modified hard sphere $H(Kn_D)$ curve applies in collision kernel calculation. Above this curve, the region bound to the left and below the lines $Kn_D = 2.5$ and $Kn_\Psi = 2.5$ is termed the high potential, near continuum regime, for which equation (18) is reasonably accurate. Outside these two regions lies the high potential, near free molecular regime, for which mean first passage time calculations can be used for collision kernel calculation, yet a single curve to calculate H is not yet determined. As mentioned in the previous section, however, collisions in the high potential, near free molecular regime are less frequent than the other two regimes, due to the correlation between high Kn_D and high Ψ_E.

IV. CONCLUSIONS

Dimensional analysis and mean first passage time calculations are used to infer the dimensionless collision kernel H as a function of both Kn_D and Ψ_E for colliding entities which interact via the Coulombic potential. Based on this study we draw the following conclusions:

1. For $\Psi_E < 0.5$ (repelling entities or weakly attracting entities), the H and Kn_D modified hard sphere curve inferred from Gopalakrishnan and Hogan[19] is excellent agreement with calculations, as are the predictions of flux matching theory[1]. At 300 K, $\Psi_E < 0.5$ corresponds to singly charged entities with a colliding radius (a_i+a_j) greater than 111 nm.

2. For cases where $\Psi_E > 0.5$, we find that the inappropriate speed and impact parameter distributions typically utilized in flux matching theory, combined with difficulties in accounting for three body trapping, lead to underprediction of the collision kernel outside the continuum limit. The alternative linear combination theory, conversely, overestimates the calculation inferred collision kernel. To determine the collision kernel under these conditions, following Gatti and Kortshagen[53] we define a potential energy based Knudsen number, Kn_Ψ, and show that for cases where the smaller of Kn_D and Kn_Ψ is less than ~2.5, H can be determined as the product of $4\pi Kn_D^2$ and a function of the smaller of Kn_D and Kn_Ψ. This enables collision kernel calculation for colliding entities in a wide size range in atmospheric pressure environments (virtually any sized singly charged particle).
3. In future work it will be necessary to find a suitable functional form to calculate collision kernels in the large Ψ_E, large Kn_D range, termed the high potential, near free molecular regime. Further, more sophisticated potential functions, and non-spherical colliding entities need to be considered. Such instances are also amenable to dimensional analysis and mean first passage time calculations[56], allowing for an appropriately defined H to be expressed as a function of Kn_D and the dimensionless parameters required to define the functional form of the potential.

ACKNOWLEDGEMENTS

We thank the Minnesota Supercomputing Institute (MSI) for providing the high performance computing hardware used in mean first passage time calculations. Partial support

for this work was provided by NSF-BES-0646507, NSF-CHE-1011810, and by the University of Minnesota Center for Filtration Research.

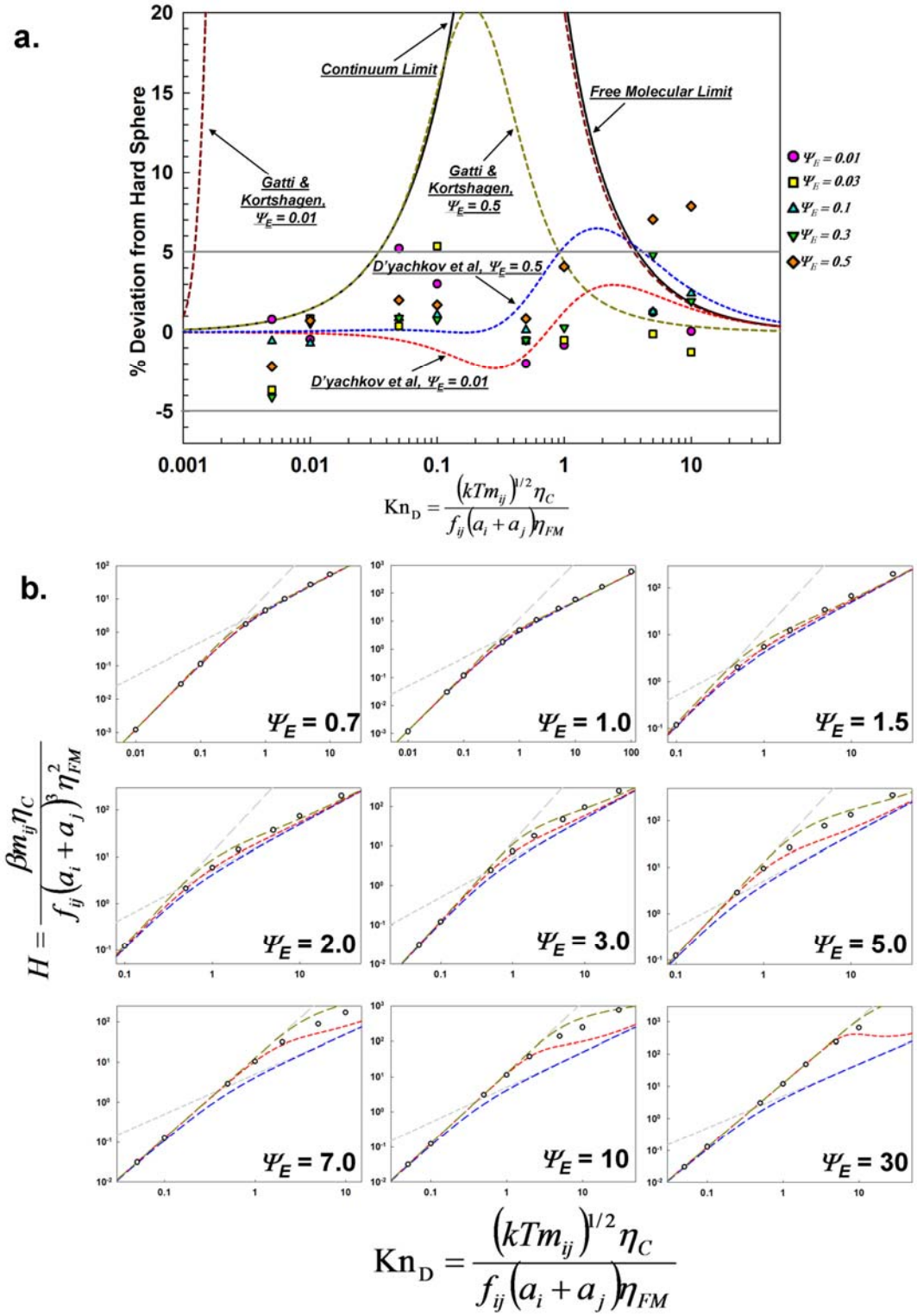

Figure 1 (a.) Results of mean first passage time calculations for attractive collisions in the $\Psi_E = 0.01$ to 0.5 range, represented by the percent deviation of calculation inferred H values from the expected hard sphere curve (equation 5). Also shown are the predictions from D'yachkov et al[52] and Gatti and Kortshagen[53]. **(b.)** $H(\mathrm{Kn_D})$ curves from mean first passage time calculations for attractive collisions in the $\Psi_E = 0.7$ to 30 range. Also plotted are the

predictions from D'yachkov et al[52] (red curve), Gatti and Kortshagen[53] (gold curve), and the previously developed hard sphere curve[19]. Dashed gray lines denote the continuum (long dash) and free molecular (short dash) expected $H(\mathrm{Kn}_D)$ curves.

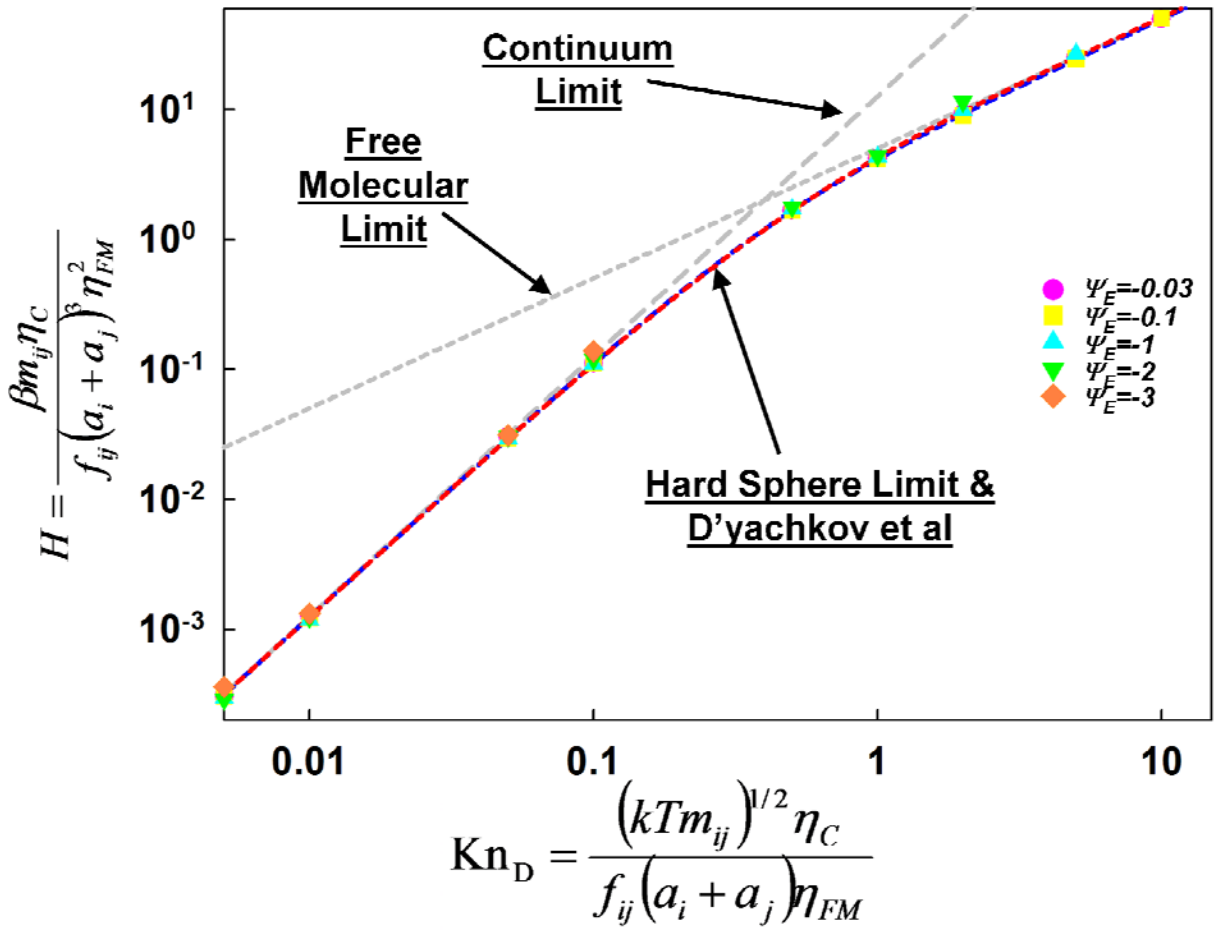

Figure 2. *H(*$\mathrm{Kn_D}$*)* curves from mean first passage time calculations for repulsive collisions in the Ψ_E = -0.03 to -3 range. Also plotted are the predictions from D'yachkov et al[52] (red curve), and the previously developed hard sphere curve (blue)[19]. Dashed gray lines denote the continuum (long dash) and free molecular (short dash) expected *H(*$\mathrm{Kn_D}$*)* curves.

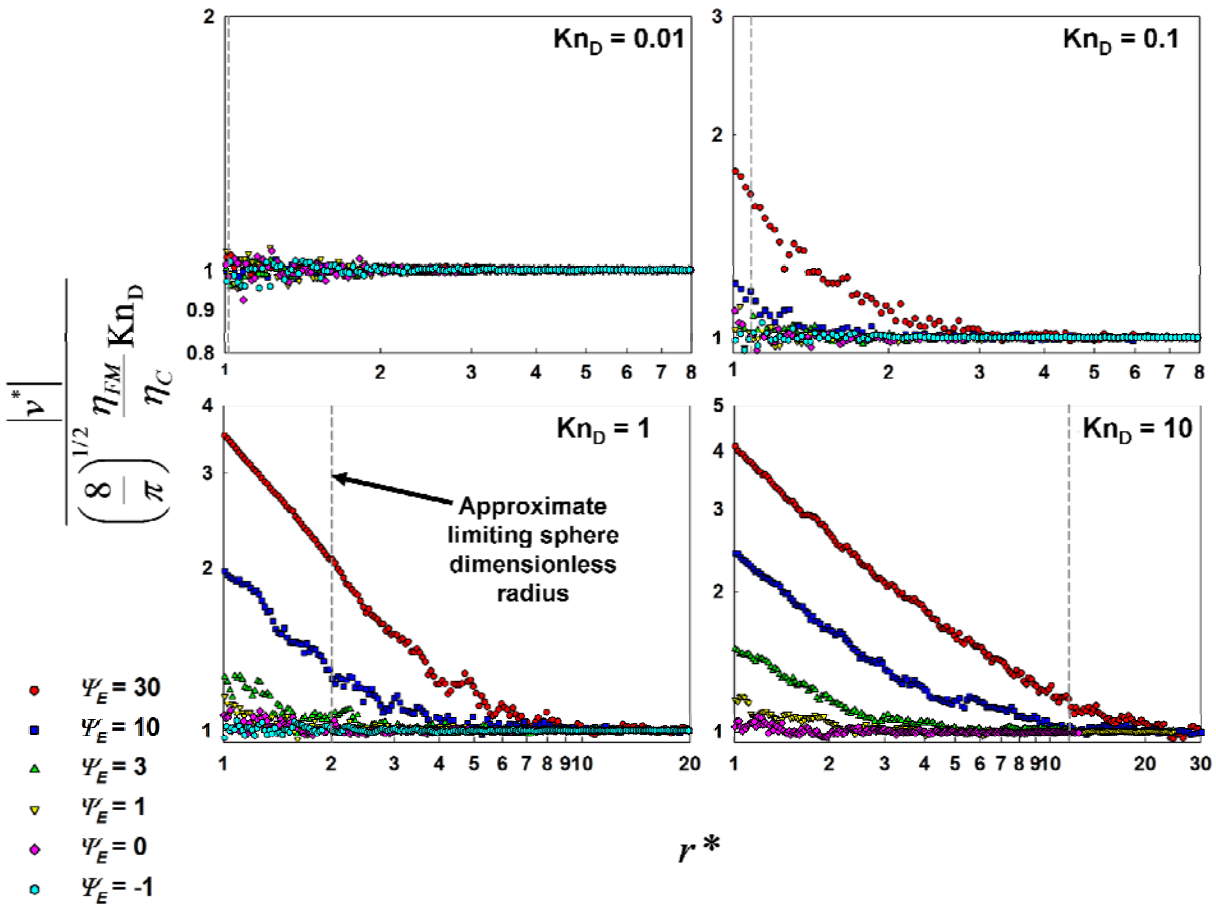

Figure 3. Normalized mean speeds of point masses in mean first passage time calculations for selected Kn_D and Ψ_E as functions of the dimensionless radial coordinate. Dashed gray lines in each graph denote the approximate dimensionless location of the limiting sphere in flux matching theory, where incoming point masses are typically assumed to have the mean thermal speed or follow a Maxwell-Boltzmann distribution.

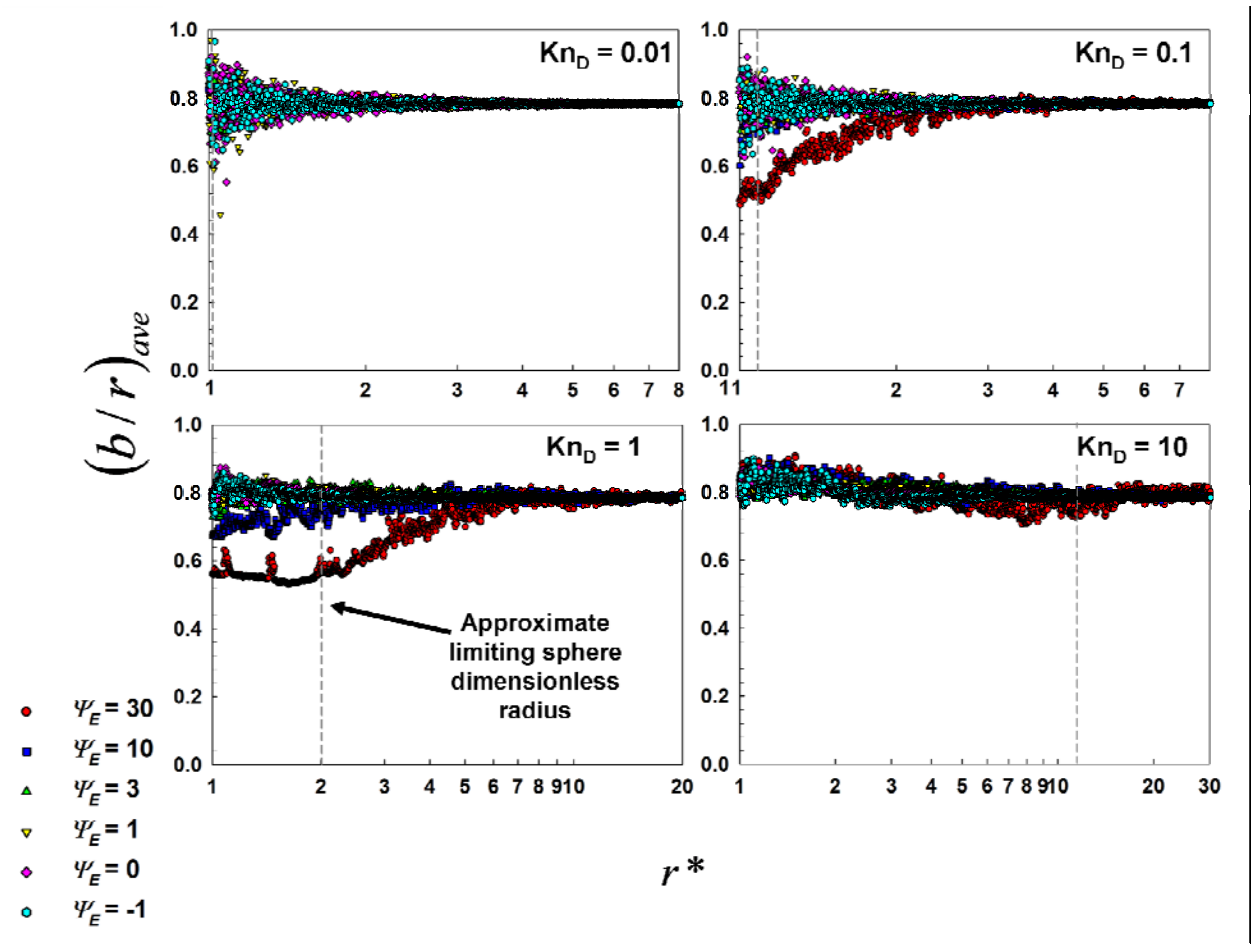

Figure 4. Mean nondimensionalized impact parameters in mean first passage time calculations for selected Kn_D and Ψ_E as functions of the dimensionless radial coordinate. Dashed gray lines in each graph denote the approximate dimensionless location of the limiting sphere in flux matching theory, where incoming point masses are typically assumed to have uniformly distributed impact parameters (mean value 0.78).

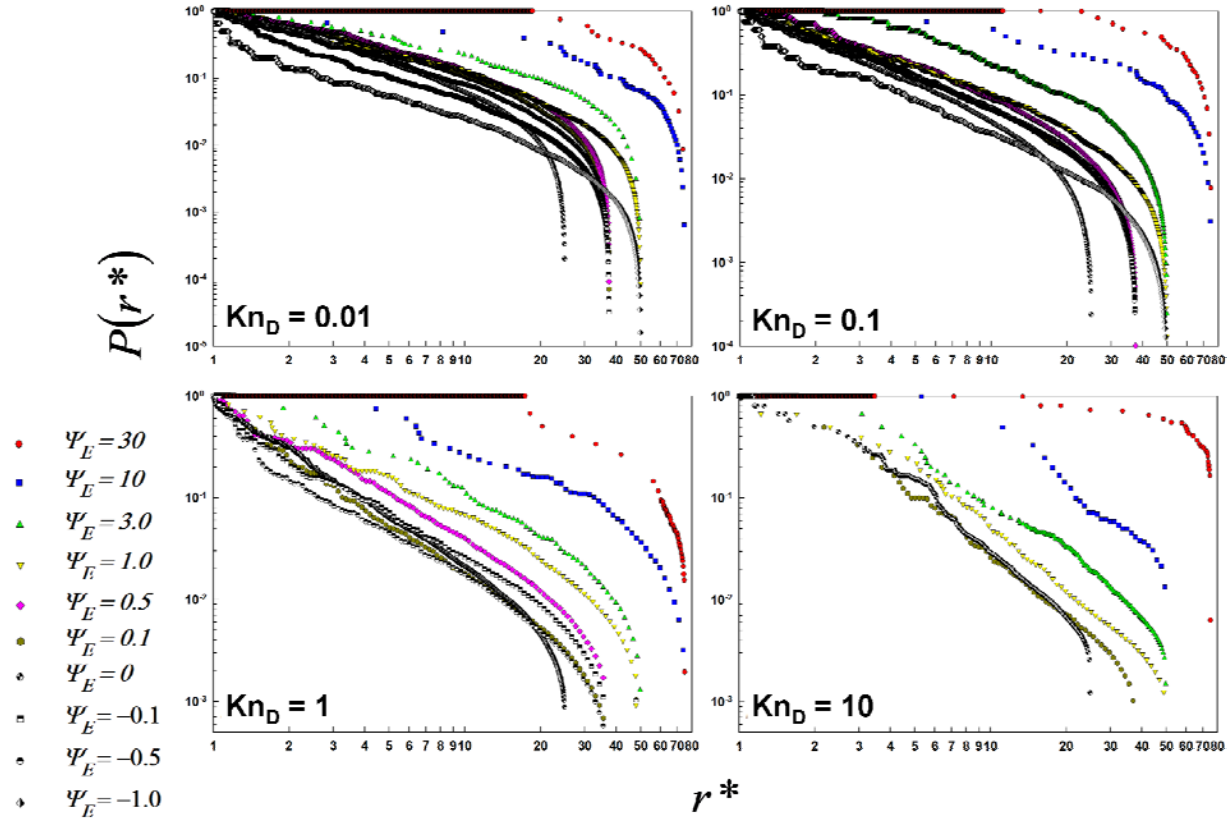

Figure 5. *P(r*)*, the probability that an incoming point mass will collide with the central sphere, as a function of the dimensionless radial coordinate, as determined from mean first passage time calculations at selected Kn_D and Ψ_E.

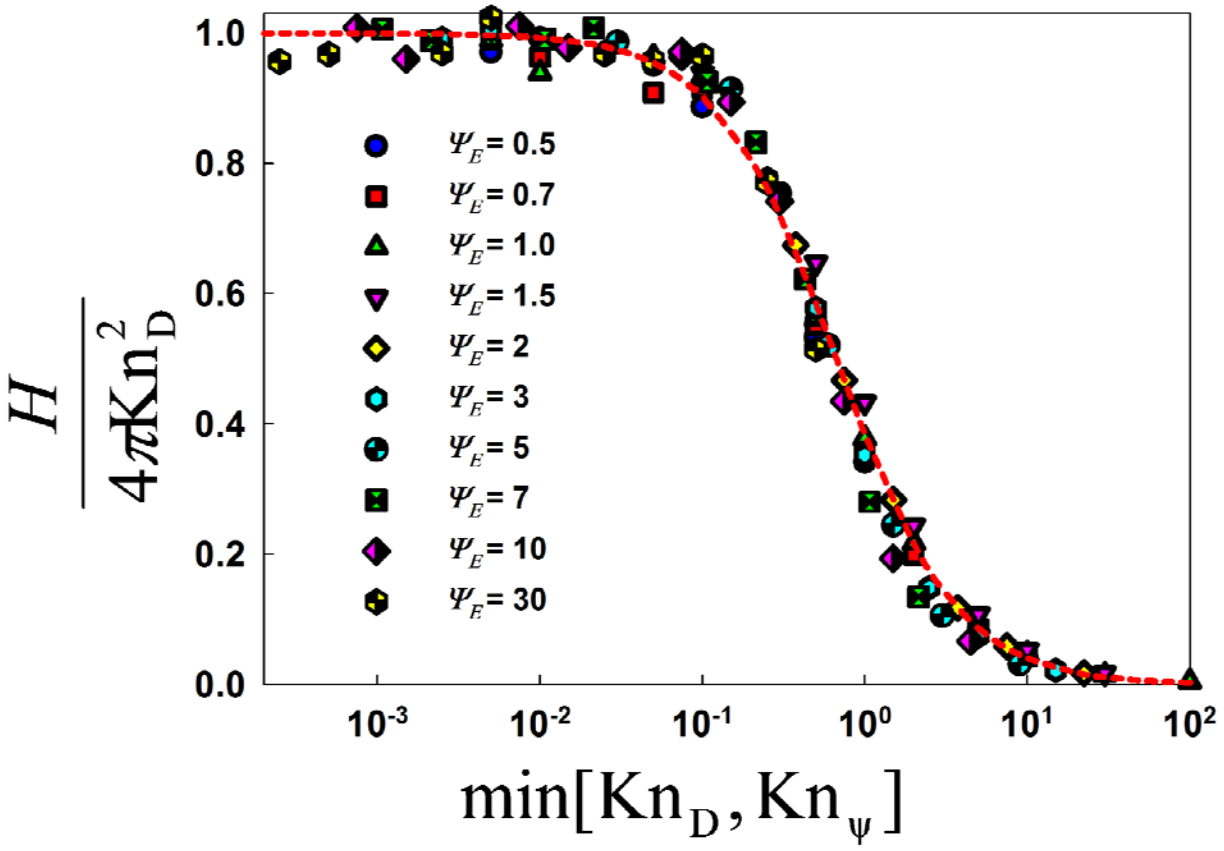

Figure 6. The ratio $H/4\pi \mathrm{Kn}_\mathrm{D}^2$ as a function of the minimum Knudsen number for a collision, either Kn_D (equation 8b) or Kn_Ψ (equation 17). The plotted dashed line denotes the regression determined curve from $\Psi_E \geq 0.5$ calculations (equation 18).

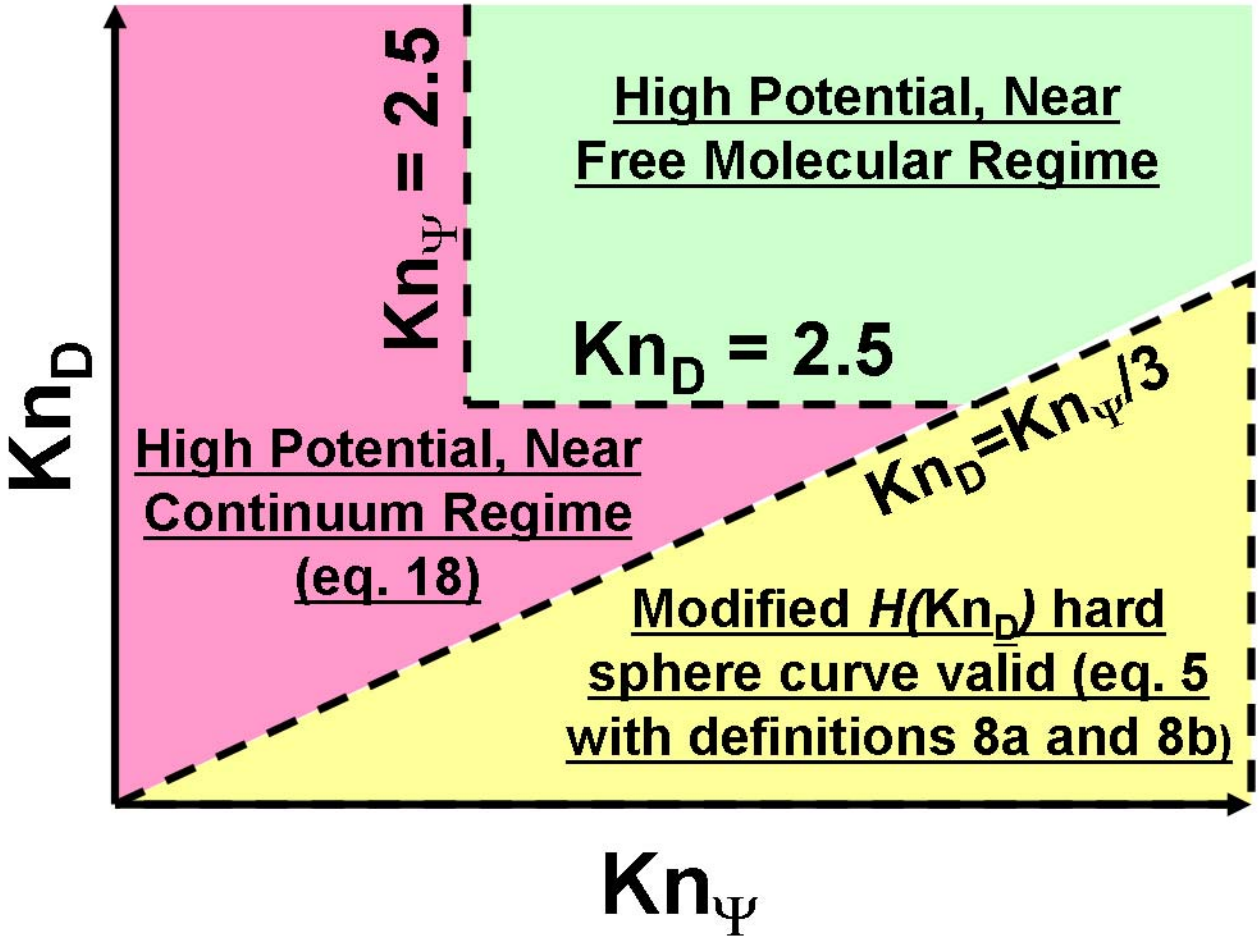

Figure 7. Phase space diagram for the calculation of the dimensionless collision kernel, dividing (Kn_D, Kn_Ψ) into three separate regimes.

REFERENCES

[1] N. A. Fuchs, Geofis. Pura Appl. **51**, 185 (1963).
[2] D. D. Huang, J. H. Seinfeld, and W. H. Marlow, Journal of Colloid and Interface Science **140**, 258 (1990).
[3] M. Adachi, Y. Kousaka, and K. Okuyama, Journal of Aerosol Science **16**, 109 (1985).
[4] J. Porstendorfer, G. Robig, and A. Ahmed, Journal of Aerosol Science **10**, 21 (1979).
[5] W. H. Marlow and J. R. Brock, Journal of Colloid and Interface Science **50**, 32 (1975).
[6] M. Michael, S. N. Tripathi, P. Arya, A. Coates, A. Wellbrock, and D. T. Young, Planetary and Space Science **59**, 880 (2011).
[7] J. K. Jiang, C. J. Hogan, D. R. Chen, and P. Biswas, Journal of Applied Physics **102**, 034904 (2007).
[8] V. Premnath, D. Oberreit, and C. J. Hogan, Aerosol Science and Technology **45**, 712 (2011).
[9] J. Goree, Physical Review Letters **69**, 277 (1992).
[10] J. Goree, Plasma Sources Science & Technology **3**, 400 (1994).
[11] L. Ravi and S. L. Girshick, Physical Review E **79**, 026408 (2009).
[12] M. Chaudhuri, S. A. Khrapak, and G. E. Morfill, Physics of Plasmas **17**, 034503 (2010).
[13] S. Khrapak and G. Morfill, Contributions to Plasma Physics **49**, 148 (2009).
[14] S. A. Khrapak, G. E. Morfill, A. G. Khrapak, and L. G. D'Yachkov, Physics of Plasmas **13**, 052114 (2006).
[15] U. Kortshagen and U. Bhandarkar, Physical Review E **60**, 887 (1999).
[16] T. Matsoukas and M. Russell, Physical Review E **55**, 991 (1997).
[17] T. Matsoukas, M. Russell, and M. Smith, Journal of Vacuum Science & Technology A-Vacuum Surfaces and Films **14**, 624 (1996).
[18] B. E. Dahneke, in *Theory of Dispersed Multiphase Flow*, edited by R. E. Meyer (Academic Press, New York, 1983).
[19] R. Gopalakrishnan and C. J. Hogan, Aerosol Science and Technology **45**, 1499 (2011).
[20] N. A. Fuchs, *The mechanics of aerosols* (Macmillan, New York,, 1964).
[21] S. K. Friedlander, *Smoke, Dust, and Haze* (Oxford University Press, New York, 2000).
[22] S. H. Northrup, S. A. Allison, and J. A. McCammon, Journal of Chemical Physics **80**, 1517 (1984).
[23] S. Chandrasekhar, Reviews of Modern Physics **15**, 1 (1943).
[24] W. H. Marlow, Journal of Chemical Physics **73**, 6284 (1980).
[25] J. E. Allen, Physica Scripta **45**, 497 (1992).
[26] W. H. Marlow, Journal of Chemical Physics **73**, 6288 (1980).
[27] A. A. Lushnikov and M. Kulmala, Journal of Aerosol Science **36**, 1069 (2005).
[28] N. A. Fuchs, Physik. Z. Sowjet. **6**, 225 (1934).
[29] G. Natanson, Soviet Physics Technical Physics **5**, 538 (1960).
[30] P. G. Wright, Discussions of the Faraday Society **30**, 100 (1960).
[31] M. S. Veshchunov, Journal of Aerosol Science **41**, 895 (2010).
[32] D. C. Sahni, Journal of Nuclear Energy **20**, 915 (1966).
[33] S. K. Loyalka, J Chem. Physics **58**, 354 (1973).
[34] D. C. Sahni, Journal of Colloid and Interface Science **91**, 418 (1983).
[35] D. D. Huang and J. H. Seinfeld, Journal of Colloid and Interface Science **139**, 213 (1990).
[36] G. Narsimhan and E. Ruckenstein, Journal of Colloid and Interface Science **107**, 174 (1985).
[37] B. Nowakowski and M. Sitarski, Journal of Colloid and Interface Science **83**, 614 (1981).
[38] A. Majerowicz, E. Pfalzmann, K. Smidovich, G. P. Reischl, W. W. Szymanski, and P. E. Wagner, Journal of Aerosol Science **21**, S39 (1990).
[39] P. E. Wagner and M. Kerker, Journal of Chemical Physics **66**, 638 (1977).
[40] W. Li and E. J. Davis, Aerosol Science and Technology **25**, 11 (1996).
[41] A. A. Lushnikov and M. Kulmala, Physical Review E **70**, 046413 (2004).

[42] W. A. Hoppel and G. M. Frick, Aerosol Science and Technology **5**, 1 (1986).
[43] A. Maisels, F. E. Kruis, and H. Fissan, Journal of Colloid and Interface Science **255**, 332 (2002).
[44] A. V. Filippov, Journal of Aerosol Science **24**, 423 (1993).
[45] G. Biskos, E. Mastorakos, and N. Collings, Journal of Aerosol Science **35**, 707 (2004).
[46] D. Y. H. Pui, S. Fruin, and P. H. McMurry, Aerosol Science and Technology **8**, 173 (1988).
[47] F. J. Romay and D. Y. H. Pui, Aerosol Science and Technology **17**, 134 (1992).
[48] G. Biskos, K. Reavell, and N. Collings, Journal of Aerosol Science **36**, 247 (2005).
[49] A. A. Kirsch and A. V. Zagnitko, Journal of Colloid and Interface Science **80**, 111 (1981).
[50] A. Wiedensohler, Journal of Aerosol Science **19**, 387 (1988).
[51] J. Bricard, Pure and Applied Geophysics **51**, 237 (1962).
[52] L. G. D'yachkov, A. G. Khrapak, S. A. Khrapak, and G. E. Morfill, Physics of Plasmas **14**, 042102 (2007).
[53] M. Gatti and U. Kortshagen, Physical Review E **78**, 046402 (2008).
[54] W. H. Marlow, Journal of Colloid and Interface Science **64**, 543 (1978).
[55] G. Klein, Proceedings of the Royal Society of London- Series A **211**, 431 (1952).
[56] R. Gopalakrishnan, T. Thajudeen, and C. J. Hogan, Journal of Chemical Physics **135**, 054302 (2011).
[57] W. G. Vincenti and C. H. Kruger, *Introduction to Physical Gas Dynamics* (Krieger, Huntington, NY, 1975).
[58] F. Pierce, C. M. Sorensen, and A. Chakrabarti, Physical Review E **74**, 021411 (2006).
[59] M. Zurita-Gotor and D. E. Rosner, Journal of Colloid and Interface Science **255**, 10 (2002).
[60] L. Isella and Y. Drossinos, Physical Review E **82**, 011404 (2010).
[61] C. N. Davies, Proceedings of the Physical Society **57**, 259 (1945).
[62] N. A. Fuchs and A. G. Sutugin, *Highly dispersed aerosols* (Ann Arbor Science Publishers, Ann Arbor, 1970).
[63] T. Matsoukas, Journal of Colloid and Interface Science **187**, 474 (1997).
[64] S. H. Northrup, M. S. Curvin, S. A. Allison, and J. A. Mccammon, Journal of Chemical Physics **84**, 2196 (1986).
[65] J. A. Given, J. B. Hubbard, and J. F. Douglas, Journal of Chemical Physics **106**, 3761 (1997).
[66] L. Isella and Y. Drossinos, Journal of Colloid and Interface Science **356**, 505 (2011).
[67] J. F. Douglas, H. X. Zhou, and J. B. Hubbard, Physical Review E **49**, 5319 (1994).
[68] D. L. Ermak and H. Buckholz, Journal of Computational Physics **35**, 169 (1980).
[69] M. S. Veshchunov, Journal of Engineering Thermophysics **20**, 260 (2011).
[70] Z. Li and H. Wang, Physical Review E **68**, 061206 (2003).
[71] G. Natanson, Zh. Tech. Fiz. **30**, 573 (1960).
[72] A. S. Amadon and W. H. Marlow, Physical Review A **43**, 5483 (1991).
[73] A. S. Amadon and W. H. Marlow, Physical Review A **43**, 5493 (1991).
[74] S. L. Girshick, P. Agarwal, and D. G. Truhlar, Journal of Chemical Physics **131**, 134305 (2009).
[75] V. A. Schweigert and I. V. Schweigert, Journal of Physics D: Applied Physics **29**, 655 (1996).
[76] S. J. Warthesen and S. L. Girshick, Plasma Chemistry and Plasma Processing **27**, 292 (2007).